LAWRENCE
LIVERMORE
NATIONAL
LABORATORY

LLNL-JRNL-844698

Global geodesic acoustic mode in an ideal magnetohydrodynamic tokamak plasma

H. J. Ren, L. Wang, D. B. Zhang, X. Q. Xu

February 1, 2023

Physics of Plasmas

Disclaimer

Global geodesic acoustic mode in an ideal magnetohydrodynamic tokamak plasma

Haijun Ren,[1,2,a)] Lai Wei,[3] Debing Zhang,[4] and X. Q. Xu[2]

[1]CAS Key Laboratory of Geospace Environment and Department of Engineering and Applied Physics, University of Science and Technology of China, Hefei, Anhui 230026, China
[2]Lawrence Livermore National Laboratory, Livermore, California 94550, USA
[3]Key Laboratory of Materials Modification by Laser, Electron, and Ion Beams (Ministry of Education), and School of Physics, Dalian University of Technology, Dalian 116024, People's Republic of China
[4]Department of Physics, East China University of Science and Technology, Shanghai 200237, China

ABSTRACT

A concise and transparent second order ordinary differential equation (ODE) describing the radial structure of the global geodesic acoustic mode (GAM) is analytically presented in a low-β tokamak plasma. The large-aspect-ratio and circular cross section are assumed to linearize the ideal magnetohydrodynamic equations. We show clearly how finite β-dependent terms affect the global GAM frequency and radial mode structure. A typical Wentzel–Kramers–Brillouin form of solution is found for some reversed shear equilibria. For some other equilibria with lower β, even also in a reversed shear tokamak, the GAM continuum is upraised by the high order β-dependent terms so that its maximum is beyond ω_G, where ω_G is the classical local frequency of GAM. As a result, no self-consistent solution to the ODE can be found.

I. INTRODUCTION

Geodesic acoustic mode (GAM) is a fundamental phenomenon existing in tokamak plasmas.[1] It plays an important role in modulating the plasma turbulence.[2–6] GAM is considered as the high frequency branch of zonal flows (ZFs) with zero toroidal and poloidal wave numbers, i.e., $m=0$ and $n=0$. A typical frequency of GAM is determined by $\frac{d}{dr}(\omega^2-\omega_G^2)\frac{d\phi_0}{dr}=0$ with $\omega_G^2=(2+1/q^2)c_s^2/R^2$, where q is the safety factor, c_s is the local sound speed, R is the major radius, and ϕ_0 is the perturbed electrostatic potential with $m=0$. There is no global mode solution unless $\frac{d\phi_0}{dr}=0$, which is of no meaning. The local dispersion relation read as $\omega^2=\omega_G^2$ leads to a continuous spectrum. It is natural for us to study the existence and radial structure of global GAM (GGAM). The GGAM was found in a reversed shear configuration plasma by the CASTOR code associated with JET experiments[7] as well as in turbulence simulations in a reversed shear tokamak.[8]

Theoretical investigation shows two ways to generate the GGAM. In the gyro-kinetic framework, taking into account second order finite-orbit-width (FOW) and the finite-Larmor-radius (FLR) effect leads to the local dispersion relation as $\omega^2=\omega_K^2+\mathcal{O}(k_r\rho_i)^2$, where k_r is the radial wave number, ρ_i is the ions' Larmor radius, and $\omega_K^2=(7/4+T_e/T_i)(2T_i/m_i)$ is the kinetic GAM frequency, in which $T_i(T_e)$ is the ions' (electrons) temperature, and m_i is the ion mass. Then replacing k_r by $-i\partial_r$ gives birth to a second order ordinary differential equation (ODE) determining the radial structure of the GAM eigenmode.[9] The other way is to consider the finite β effect in the fluid framework. So, the $m=0$ component of the perturbed electrostatic potential and $m=\pm2$ sideband can be coupled together.[10–12]

Most of the previous work related to the radial structure and global mode of GAM in the fluid frame is based on the vortex equation and current quasi-neutrality condition $\nabla\cdot\delta\vec{J}=0$, where $\vec{J}$ is the plasma current.[13,14] For example, in an excellent analytical work,[11] Kolesnichenko *et al.* (hereinafter PPCF2013) presented the ODE for GGAM. But its expression is not concise enough. It is difficult to show which term plays a key role in the formation of GGAM, and which term can be safely eliminated. Also, as pointed out in Ref. 15, since $\vec{J}=\nabla\times\vec{B}$ (in the low-frequency approximation) has been used in the linearization of the ideal MHD equation, which is an enclosed system, there is no need to introduce an additional equation to derive the linear dispersion relation or the final ODE. Reference 10 used the vortex equation and the current quasi-neutrality condition along with the MHD equations, and Ref. 12 used extremely complicated ordering

analysis to derive the ODE, which was presented as the 94th equation in their paper.

Early in 2008, Wahlberg performed a second order ODE describing the harmonics by solving the Frieman–Rotenberg eigenvalue equation in the presence of toroidal rotation, but focused on the effect of toroidal rotation on the local GAM frequency.[16] In his following work cooperated with Graves,[17] the ideal MHD theory is used to investigate some fundamental properties of the geodesic acoustic continuum modes in tokamaks, including their global structure, their associated magnetic components both inside and outside the plasma, and the effects of a non-circular cross section of the plasma. In a recent work,[18] with the help of the ordering analysis method, Wahlberg and Graves extended their MHD analysis in Ref. 17 to calculate additional components of GAM which exist outside the GAM surface in shaped tokamaks. However, they did not pay much attention to the global structure of GAM and the eigenfrequency of GGAM.

In the present work, starting from the linearized ideal MHD equations, we present a concise and straightforward derivation for the ODE determining the radial structure of $\delta\phi_2$, the $m=2$ component of the perturbed electrostatic potential. The mode equations describing ϕ_0 and ϕ_2 and the ODE presented in this work show their difference from the results reported in Refs. 10–12. The difference is illustrated in detail and it is explained how the discrepancies come into being. Our results clearly imply that some high-order terms can play a significant role in the generation of GGAM. The rest of the present work is organized as follows: Sec. II is devoted to the linear derivation. The final two mode equations and ODE are presented. Section III is the detail discussion about the eigenfrequency and mode structure of the GGAM for different equilibrium profiles. Finally, the conclusion is given in Sec. IV.

II. CONCISE DERIVATION

Let us start our derivation from the ideal MHD equations, which read

$$\partial_t p + c_s^2\rho\nabla\cdot\vec{u} + \vec{u}\cdot\nabla p = 0, \tag{1}$$

$$\rho\frac{d\vec{u}}{dt} = -\nabla p + (\nabla\times\vec{B})\times\vec{B}, \tag{2}$$

$$\partial_t\vec{B} = \nabla\times(\vec{u}\times\vec{B}). \tag{3}$$

Here, p, ρ, $\vec{u}$, and $\vec{B}$ are the pressure, plasma mass density, fluid velocity, and magnetic field, respectively. The magnetic constant μ_0 (as well as Boltzmann constant k_B below) is omitted for simplicity of notation. In order to linearize these equations, we consider a large-aspect-ratio tokamak plasma with a toroidally symmetric magnetic field $\vec{B} = I(\psi)\nabla\zeta + \nabla\zeta\times\nabla\psi$ and work in the (r,θ,ζ) coordinate system, where $\psi(r)$ is the magnetic flux, and θ and ζ are the toroidal and poloidal angles, respectively. A circular cross section is assumed in our calculation with $R = R_0 + r\cos\theta$ with $\epsilon = r/R_0 \ll 1$ and a low-β condition is adopted. The prefix δ denotes the perturbed profile. The displacement $\vec{\xi}$ is expanded into $\xi_r\nabla r + \xi_\parallel\vec{B}/B + \xi_\theta\vec{B}\times\nabla r/B$. Keeping the terms to the leading order, we obtain the following linearized equations:

$$\delta p = -c_s^2\rho\varphi - p'\xi_r, \tag{4}$$

$$\delta B_r = B\nabla_\parallel\xi_r, \tag{5}$$

$$\delta B_\theta = \nabla_\parallel(B\xi_\theta) + \chi\xi_r, \tag{6}$$

$$\delta B_\parallel = -B\left(\varphi + 2\mathcal{K}_\theta\xi_\theta + 2\mathcal{K}_r\xi_r + \frac{c_s^2\nabla_\parallel^2}{\omega^2}\varphi - \frac{p'}{B^2}\xi_r\right), \tag{7}$$

$$-\rho\omega^2\xi_\theta = -\frac{1}{r}\partial_\theta\delta P + J_\parallel\delta B_r + B^2\nabla_\parallel(\delta B_\theta/B) + 2\mathcal{K}_\theta(\delta P + c_s^2\rho\varphi + p'\xi_r), \tag{8}$$

$$-\rho\omega^2\xi_r = -\frac{\partial\delta P}{\partial r} - (J_\parallel + \chi)\delta B_\theta + B\nabla_\parallel\delta B_r + 2\mathcal{K}_r(\delta P + c_s^2\rho\varphi + p'\xi_r). \tag{9}$$

Here, φ stands for $\nabla\cdot\vec{\xi}$, $\mathcal{K}_\theta$ is the geodesic component of the magnetic curvature $\vec{\mathcal{K}}$ defined as $(\vec{B}/B\cdot\nabla)\vec{B}/B$, and $\mathcal{K}_r$ is the radial component of $\mathcal{K}$. χ is short for $\frac{\psi'}{BR^2}\nabla\psi\cdot\nabla(I/\psi') + \frac{I}{B}\nabla\cdot(R^{-2}\nabla\psi) - \frac{I\nabla r\cdot\nabla\psi'}{BR^2}$, which can be simplified to $\frac{B_0}{qR_0}s$. Here, $s = d\ln q/d\ln r$ is the magnetic shear. $J_\parallel$ is the parallel equilibrium current, defined as $J_\parallel = \frac{I}{B}\nabla\cdot(R^{-2}\nabla\psi) - I'\psi'/(BR^2)$. The prime denotes the derivative to the minor radius r. Generally to the leading order, we can assume $J_\parallel \simeq \frac{B_0}{qR_0}\eta$, where the subscript 0 denoted the value at $r=0$, namely, on the magnetic axis. $\delta P = \delta p + B\delta B_\parallel$ represents the total perturbed pressure. The parallel displacement $\xi_\parallel = -\frac{c_s^2\nabla_\parallel\varphi}{\omega^2}$ is adopted in Eq. (7). $c_s^2 = \Gamma p/\rho$ is the local sound speed with an adiabatic index Γ.

A typical assumption used for GAM is $\delta P \simeq 0$, in order to eliminate the coupling with a fast magnetosonic wave (FMW). That means in the reduced MHD equations, we have[13]

$$\left(1 + \frac{c_s^2\rho}{B^2} + \frac{c_s^2\nabla_\parallel^2}{\omega^2}\right)\varphi + 2\mathcal{K}_\theta\xi_n + 2\mathcal{K}_r\xi_r = 0. \tag{10}$$

According to Eqs. (6) and (7), it is reasonable to assume

$$B\xi_\theta = B_0\xi_n. \tag{11}$$

The second mode equation is often derived from the current quasi-neutrality condition,[11,13,14] and normally ordering analysis is used by dropping high order terms.[13] Here, we use Eqs. (8) and (9) to eliminate their first terms on the right-hand side, then we arrive at

$$\begin{aligned}
&\frac{\partial}{\partial r}\left(-\frac{\omega^2R_0^2}{v_A^2}r\xi\right)_n + \frac{\omega^2R_0^2}{v_A^2}\partial_\theta\xi_r - \frac{\partial}{\partial r}\left(2\sin\theta\frac{c_s^2}{v_A^2}rR_0\varphi\right) - \partial_\theta\left(2\cos\theta\frac{c_s^2}{v_A^2}R_0\varphi\right)\\
&= \frac{\partial}{\partial r}\left(\frac{r}{q^2}\partial_\theta^2\xi_n\right) + \frac{\eta+s}{q^2}\partial_\theta^2\xi_n + \frac{\partial}{\partial r}\left(\frac{r}{q^2}(\eta+s)\partial_\theta\xi\right)_r + (\eta+s)\frac{s}{q^2}\partial_\theta\xi_r - \frac{1}{q^2}\partial_\theta^3\xi_r\\
&\quad + \frac{\partial}{\partial r}\left(2rR_0\sin\theta\frac{p'}{B_0^2}\xi_r\right) + \partial_\theta\left(2R_0\cos\theta\frac{p'}{B_0^2}\xi_r\right),
\end{aligned} \tag{12}$$

where $v_A^2 = B_0^2/\rho$ is the Alfvén velocity. Recall again that B_0 is the magnetic field on the magnetic axis, while the density $\rho = \rho(r)$ is the local one.

In the low-β ($\beta \ll 1$) condition, the leading order terms of Eq. (10) are

$$\left(1+\frac{c_s^2\nabla_\parallel^2}{\omega^2}\right)\varphi+2\mathcal{K}_\theta\xi_n=0. \tag{13}$$

Recalling that φ is defined as $\nabla\cdot\vec{\xi}$, we find $\varphi=\nabla\cdot\vec{\xi}_\perp-c_s^2/\omega^2\nabla_\parallel^2\varphi$. On the other hand, there is

$$\nabla\cdot\vec{\xi}_\perp=\frac{1}{r}\frac{\partial}{\partial r}(r\xi_r)-2\mathcal{K}_\theta\xi_n+\frac{1}{r}\partial_\theta\xi_n. \tag{14}$$

It is easy to find that

$$\frac{\partial}{\partial r}(r\xi_r)=-\partial_\theta\xi_n. \tag{15}$$

A general set of non-trivial solutions to the equation above is $\xi_n=\frac{\partial\phi}{\partial r}$ and $\xi_r=-\frac{1}{r}\partial_\theta\phi$.

For simplicity of notification, let us introduce the normalized frequency $\bar{\omega}=\omega R_0/c_{s0}$, the normalized temperature $\bar{T}(r)=c_s^2/c_{s0}^2$, and $\beta(r)=\Gamma p/B_0^2$ depending on the magnetic flux via $p(r)\equiv\rho(r)T(r)$. The overlines of $\bar{T}$ and $\bar{\omega}$ are omitted below without causing confusion. Meanwhile, $\varphi_s=R_0\varphi$ is defined, and $\mathcal{K}_\theta=\sin\theta/R_0$ and $\mathcal{K}_r=-\cos\theta/R_0$ are adopted. Generally for GAM, we consider the sideband couplings of ϕ_0 and $\phi_{\pm2}$,[19,20] where $\phi=\sum_m\phi_m e^{im\theta}$ is assumed, and simply suppose $\phi_m=0$ for odd number m. As a result, we can ignore the last two terms in Eq. (12). By substituting ξ_n and ξ_r into Eqs. (10) and (12), we obtain the following two equations:

$$\left(1+\beta+\frac{T}{\omega^2q^2}\partial_\theta^2\right)\varphi_s=-2\sin\theta\frac{d\phi}{dr}-2\cos\theta\frac{1}{r}\partial_\theta\phi, \tag{16}$$

$$\begin{aligned}&\frac{d}{dr}\left(-\omega^2r\beta T^{-1}\frac{d\phi}{dr}\right)-\frac{d}{dr}(2\beta r\varphi_s\sin\theta)-\partial_\theta(2\beta\varphi_s\cos\theta)\\&=\frac{d}{dr}\left(\frac{r}{q^2}\frac{d}{dr}\partial_\theta^2\phi\right)+\frac{1}{r}\left(\omega^2\beta T^{-1}-\frac{s(\eta+s)}{q^2}\right.\\&\left.-r\frac{d}{dr}\left(\frac{\eta+s}{q^2}\right)+\frac{1}{q^2}\partial_\theta^2\right)\partial_\theta^2\phi.\end{aligned} \tag{17}$$

For $m=0$ and $m=2$, the two equations above yield the following two mode equations as

$$(\omega^2-\omega_G^2)\frac{d\phi_0}{dr}+\frac{T}{1+\beta}\left(2\frac{d\phi_2}{dr}+\frac{4\phi_2}{r}\right)=0, \tag{18}$$

and

$$\begin{aligned}&\frac{d}{dr}\left[\frac{1}{q^2}-\frac{\omega^2\beta T^{-1}}{4}+\frac{\beta(G_1^{-1}+G_3^{-1})}{4}\right)r\frac{d\phi_2}{dr}\Bigg]\\&-\frac{1}{4}r^2\frac{d}{dr}\left(\frac{\beta}{r}G_1^{-1}\frac{d\phi_0}{dr}\right)+\frac{1}{r}\left\{\omega^2\beta T^{-1}+\frac{1}{q^2}[(\eta+s)s-4]\right.\\&\left.-\frac{r}{q^2}(\eta+s)'-\beta(G_1^{-1}+G_3^{-1})+\frac{r}{2}\left[\beta(G_1^{-1}-G_3^{-1})\right]'\right\}\phi_2=0,\end{aligned} \tag{19}$$

respectively. Here, $\omega_G^2=(2+\frac{1}{q^2})T/(1+\beta)$ is the local normalized GAM frequency with modification of finite β.[15,19] The local frequency depends on the minor radius r, leading to the continuous spectrum of GAM. G_m stands for $1+\beta-m^2T/(\omega^2q^2)$. Zeroing it leads to the toroidal acoustic modes (TAM) frequency $\omega_{Tm}=\sqrt{m^2T/(q^2(1+\beta))}$ with poloidal wave number m. We have adopted the $\beta q^2\ll1$ condition to cut off the coupling chains, i.e., $\phi_{\pm4}\sim0$ since there is $\phi_{\pm4}\sim(\beta q^2)^2\phi_0$. The two equations above describe the radial structure and the global mode of GAM in an ideal MHD framework by taking into account the finite β effect. Equation (18) reminds us that if we assume $\phi_N\equiv r^2\phi_2$, the two mode equations can be simplified to

$$(\omega^2-\omega_G^2)\frac{d\phi_0}{dr}+\frac{2T}{(1+\beta)r^2}\frac{d\phi_N}{dr}=0, \tag{20}$$

as well as

$$\begin{aligned}&\frac{d}{dr}\left[\frac{1}{r^3}\quad\frac{1}{q^2}-\frac{\omega^2\beta T^{-1}}{4}+\frac{\beta(G_1^{-1}+G_3^{-1})}{4}\right)\frac{d\phi_N}{dr}\Bigg]\\&-\frac{1}{4}\frac{d}{dr}\left(\frac{\beta}{r}G_1^{-1}\frac{d\phi_0}{dr}\right)+\frac{1}{r^5q^2}\left[(\eta+s+4)s-r(\eta+s)'\right.\\&\left.+\frac{r}{2}q^2\frac{d}{dr}(\beta\omega^2T^{-1}-2\beta G_3^{-1})\right]\phi_N=0.\end{aligned} \tag{21}$$

The finite β is shown to play a crucial role in the sideband coupling. When zeroing β, there is only a trivial solution with $\phi_0=$ const and $\phi_2=0$, which is of no interest and will not be discussed here. By inserting Eq. (20) into Eq. (21), we finally obtain the second order ODE describing the radial structure of the $m=2$ harmonic of the GAM potential:

$$\begin{aligned}&\frac{d}{dr}\left[\frac{1}{r^3}\left(\frac{1}{q^2}+\frac{1}{4}\beta_s\frac{\omega^2}{\omega^2-\omega_G^2}+\boxed{\frac{\beta}{4G_3}-\frac{\omega^2\beta T^{-1}}{4}}\right)\frac{d\phi_N}{dr}\right]\\&+\frac{1}{r^5q^2}\left\{(\eta+s+4)s-r(\eta+s)'\right.\\&\left.+\boxed{rq^2\frac{d}{dr}\left[\beta(\omega^2T^{-1}/2-G_3^{-1})\right]}\right\}\phi_N=0.\end{aligned} \tag{22}$$

Here, β_s is short for $\frac{\beta}{1+\beta}$. As discussed in Ref. 12 (hereinafter as NF2018), ω_G forms a continuous spectrum. At least, we can find a point $r=r_0$, at which $\omega=\omega_G(r_0)$ is satisfied. Only in the region near r_0, one has $\omega^2-\omega_G^2\sim\mathcal{O}(\beta)$, so the second term in the first bracket of the equation above can be compared to $1/q^2$. In the region far away from r_0, $\omega^2-\omega_G^2\sim\mathcal{O}(1)$ could come into being due to the radial profile of T and q. As a result, ϕ_0 tends to be flat (namely, $d\phi_0/dr$ is small).[11] The boxed terms are formally of higher order than other terms and will be specifically discussed in Sec. III.

III. DISCUSSION

We point out that the first mode equation (20) here is the same as the one in Ref. 10 (Hereinafter as PPCF2014) [see Eq. (17) and note that their Φ_2 equals our $2\phi_N$]. But the second mode equation (21) [or the final one Eq. (22)] is not identical with its analog in PPCF2014. When the $G_3^{-1}-$ dependent term is disregarded, β_s is abbreviated as β, the second boxed term is neglected, and $\eta=0$ is adopted, our result is reduced to the one in PPCF2014. Indeed, even the G_3 term may be safely ignored since it is much less than other terms, and β_s can be directly replaced by β without loss of importance. However, $\eta=0$ means $J_\parallel=0$. This is not a realistic assumption in a large-aspect-ratio tokamak in the limit of a circular cross section, even it has been adopted in Refs. 10, 14, and 21. This assumption will dramatically reduce the efficiency and applicability of the ODE since generally, there is $\eta=2-s$.

When we let $\eta + s = 2$ and neglect the two boxed terms in Eq. (22), NF2018's result [see Eq. (94) in NF2018] is exactly recovered. It costed almost ten pages and more than 90 equations in NF2018 to derive the ODE by using complicated ordering analysis, and eventually only the leading order terms were presented. As mentioned above, only in the small region of $r \sim r_0$, the second term in the first bracket of the above equation can be of order $\mathcal{O}(1)$. In the region far away from r_0, this term is of the same order as the first boxed term. As a result, the absence of the first boxed term may induce some discrepancy. Besides, due to the fact that ω_{T3} can be comparable to ω_G in some cases, the effect of β/G_3 term may be of great importance.

Equation (19) shows that ϕ_2 is of the order $\beta q^2 \phi_0$. And therefore, the higher order harmonics are ignorable ($\phi_m = \beta^{m/2} q^m \phi_0$) for even number m. ϕ_2 plays a key role in generating the global mode. The other factor is the FLR effect, which is considered in the gyrokinetic framework,[9] but not taken into account here. Although G_1 seems to be a singularity in the mode equation (21), it can be eliminated in the ODE (22). That means there is no global mode for the TAM. Furthermore, PPCF2014 used the vortex equation and the current quasi-neutrality condition $\nabla \cdot \delta J = 0$ to derive the mode equations, as done in Ref. 11 (hereinafter PPCF2013). The ODE in PPCF2013 [see Eq. (64)] is not as transparent as our result Eq. (22), but detail analysis shows that after removing the term $(1 - 1/q^2) r \beta'$, Eq. (64) in PPCF2013 is identical with our result. Let us again pay attention to Eq. (17). When we set $\omega = 0$ and hence $\varphi_s = 0$ according to Eq. (16), the equation is simplified to $(r\phi_m'/q^2)' - (2s + m^2)\phi_m/(rq^2) = 0$. There is no possibility that a term related to β' can be generated here. However, that term has only tiny quantitative effect on the eigenfrequency and mode structure and consequently, can always be disregarded safely.

A. Case for $\beta(0) = 0.01$

As pointed out in PPCF2013, the GGAM with a reversed-shear configuration was found by the CASTOR code in Ref. 7. PPCF2013 showed that in the presence of energetic ions, the GAM continuum can have a maximum even when $q(r)$ and the radial profiles of plasma parameters are monotonic, which eventually leaded to a GGAM. Here, due to the lack of energetic ions or other non-ideal dissipative effects, we do not consider the energetic-particle-induced GAM (EGAM) and follow PPCF2013 to use the similar equilibrium profiles by restricting ourselves to the reversed-shear condition, as shown in Fig. 1.

Let us focus on the coefficient of ϕ_N'' term in the ODE. Due to the presence of the boxed term, the coefficient is rewritten as

$$\alpha \frac{(\omega^2 - O_3^2)(\omega^2 - O_2^2)(\omega^2 - O_1^2)}{(\omega^2 - \omega_G^2)(\omega^2 - \omega_{G3}^2)}. \tag{23}$$

Here, α represents other terms in the coefficient, O_3 is the continuum related to $\omega^2 \beta T^{-1}/4$ with the greatest frequency $> \omega_G$, corresponding to the no global mode. O_1 is the continuum introduced by the term β/G_3 with $\omega_{T3}^2 = 9T/[q^2(1+\beta)]$. Both O_1 and O_3 do not exist in NF2018 since the boxed terms are ignored. As illustrated in Fig. 2, O_2 is the GAM continuum and its analog is mode O in the case without boxed terms. For convenience of discussion, let us define case A with the boxed terms and case B without the boxed terms here. It is not surprising that O_2 is reduced to $O = \omega_G/\sqrt{(1 + q^2\beta_s/4)}$ without the boxed terms. Figure 2 also shows ω_1^A and ω_1^B have tiny differences

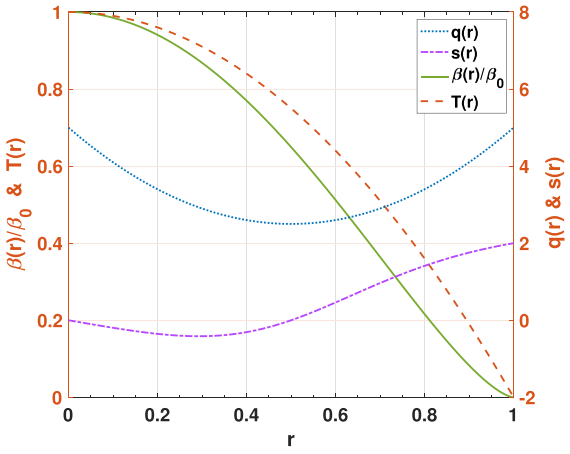

FIG. 1. Equilibrium profiles for case A and B: $\beta(r) = \beta(0)(1 - r^2)^{\frac{3}{2}}$ with $\beta(0) = 0.01$, $q(r) = 10(r - 0.5)^2 + 2.5$, $T(r) = 1 - r^2$. Here, r is normalized by the minor radius.

with each other, where $\omega_1^{A(B)}$ is one of the eigenfrequencies of GGAM for case A(B).

The radial structures of ϕ_2, ϕ_0, and ϕ_0' for different eigenfrequencies of GGAM are shown in Fig. 3. The results in case A and in case B are plotted together to make a comparison. Figure 3 implies clearly that although the high order boxed term introduces O_1 and O_3 continuums, it has a trivial effect on the GGAM. Curves for case A have only ignorable quantitative discrepancy with the curves for case B.

B. Case for $\beta(0) = 0.001$

The boxed terms, or more specifically, the first boxed term in the ODE cannot be disregarded in all cases, whereas the second boxed

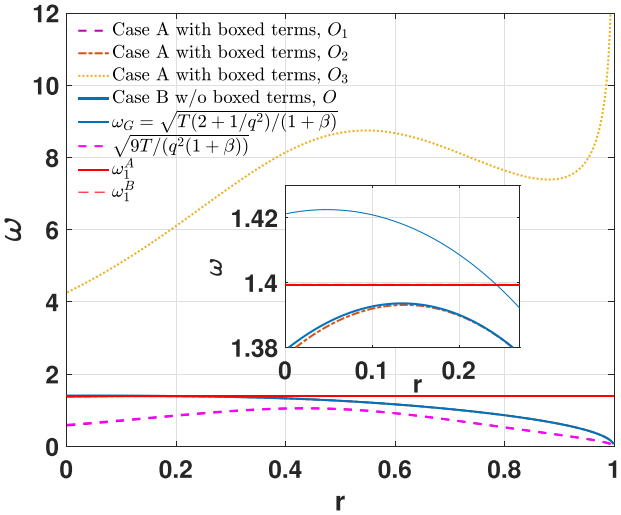

FIG. 2. Eigenfrequencies and different branches of continuums. $\omega_1^A = 1.3993$ and $\omega_1^B = 1.3995$ are almost the same.

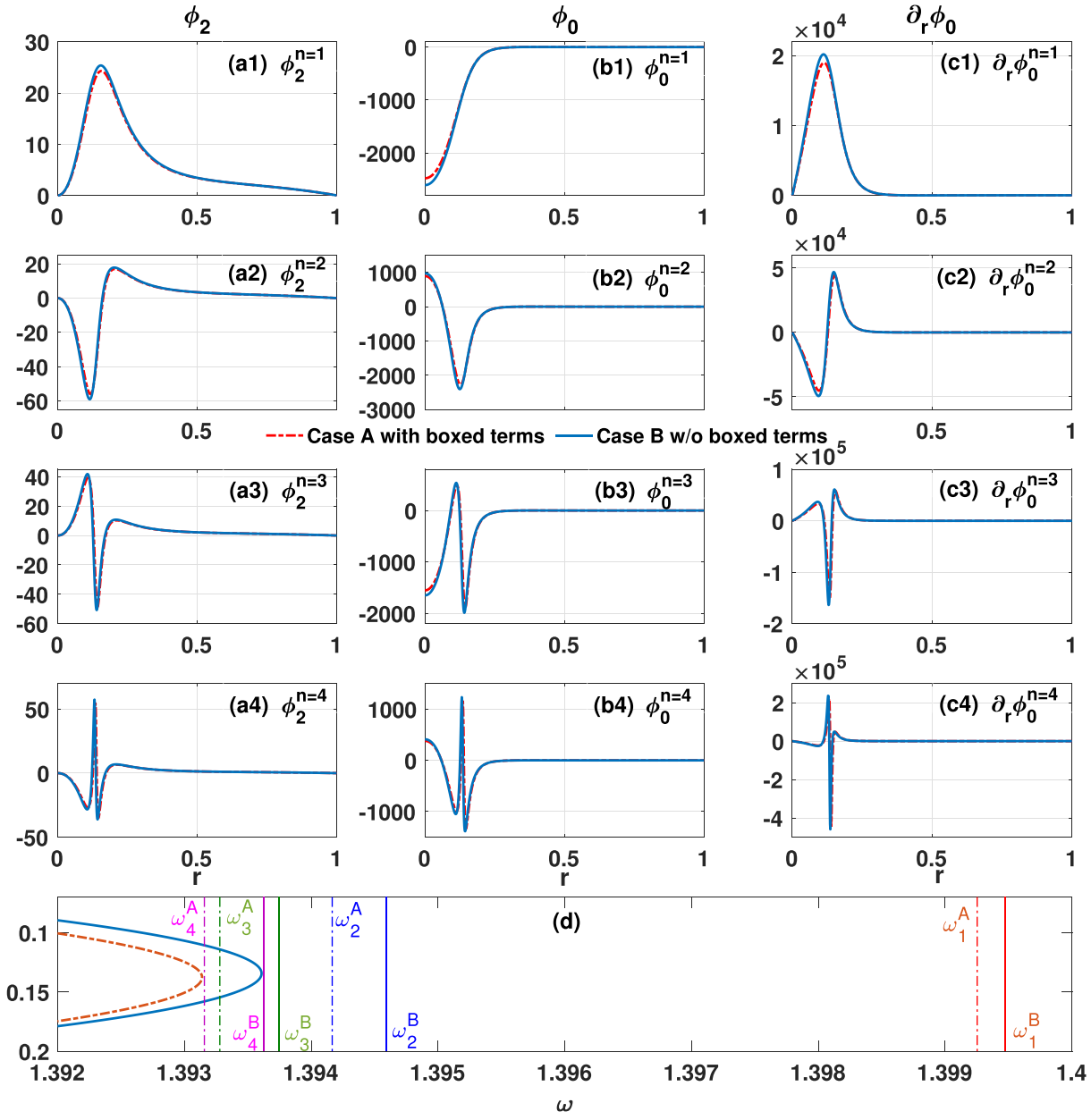

FIG. 3. The radial structures of ϕ_2, ϕ_0, and ϕ_0' (i.e., the $m=0$ component of the radial electric field E_r) are displayed for case A and B. n represents the number of turning points of the curves. PPCF2013 considered only $n=1$ and $n=2$ cases with different β. The bottom plot shows that the less the distance between the eigenfrequency and the continuum O_2/O is, the larger n is, or the larger the radial wavenumber k_r is.

term is ignorable. The role of the boxed term varies with the equilibrium profiles. The ODE (22) can be simply written as $(a\phi_N')' + b\phi_N = 0$. After making the transfer $f = \sqrt{a}\phi_N$, the ODE can be re-expressed in a standard form, $f'' + cf = 0$ with $c = \frac{b+(a')^2/(4a)-a''/2}{a}$. Numerical evaluation shows that for the GGAM with equilibrium profiles displayed in Fig. 1 and an eigenfrequency in Fig. 3, c is almost positive in all the regions. So the ODE will have a local Wentzel–Kramers–Brillouin (WKB) solution with $k_r \sim \sqrt{c}$. Meanwhile we note that c is almost proportional to $1/(\omega^2 - O^2)$. Hence, the smaller $\omega - O$ is, the larger c, *viz.* the larger k_r is. In the

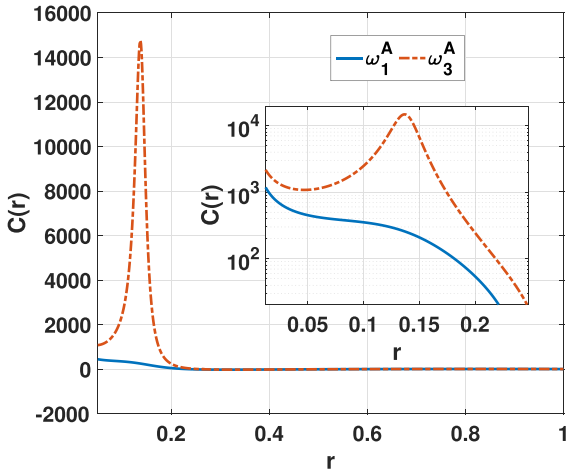

FIG. 4. The radial distribution of the value of c. In most regions, c is positive. In the region of $r < r_0$, c for $n = 3$ is higher than the one for $n = 1$ by almost two orders.

outer region $r > r_0$, c is relatively small, meaning long wavelength. These are all confirmed by Figs. 3 and 4. When the equilibrium profile is changed to make c negative in most of the region away from r_0, the mode structure will be remarkably different. Figure 5 shows the equilibrium profile considered in NF2018. When the boxed terms are disregarded, the mode structure is plotted in Fig. 6, in which the eigenfrequency $\omega_{eig} = 1.4895$ is used as shown in Fig. 7. The left-top plot in Fig. 6 also can be found in NF2018 (see Fig. 2 in NF2018). The value of the term c is shown in the bottom plot. Just as discussed above, in the region away from r_0, c is negative, leading to the exponential distribution. As a result, the spatial scale length of the mode for ϕ_2 seems to

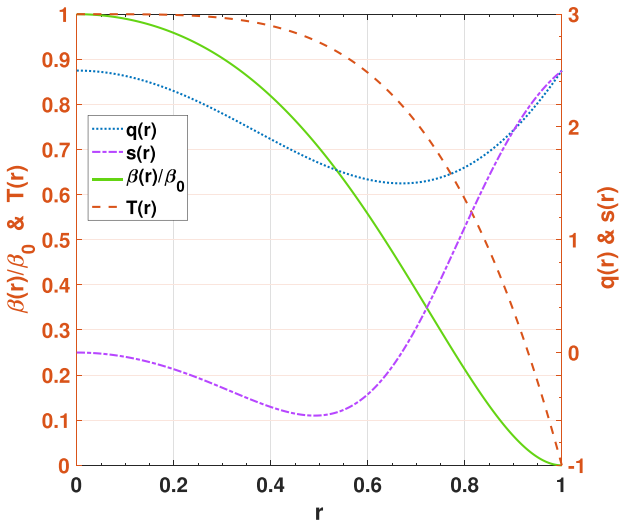

FIG. 5. Equilibrium profiles for case C (with boxed terms) and D (without boxed terms): $\beta = \beta(0)(1-r^2)(1-r^4)$ with $\beta(0) = 0.1\%$, $T = 1 - r^4$, $q = -1.67r^6 + 6.64r^4 - 4.79r^2 + 2.5$.

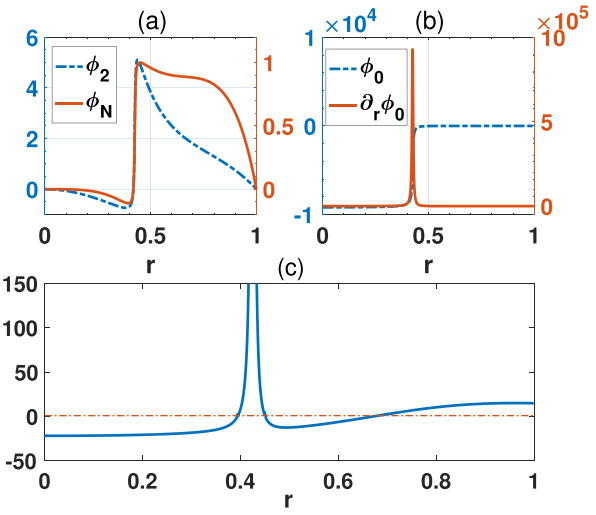

FIG. 6. The radial structure of ϕ_2, ϕ_N, ϕ_0, and ϕ_0' is plotted, and the value of term c is evaluated for case D.

be much greater than the one in Fig. 3. However, NF2018 did not pay any attention to ϕ_0 and ϕ_0'. As shown in the right-top plot in Fig. 6, ϕ_0' has an extremely narrow structure with a sharp peak basically around r_0.

After we take into account the boxed terms, the result will be remarkably changed. In fact, we cannot find a self-consistent eigenfrequency and a corresponding global mode. It is due to the presence of the boxed terms, the GAM continuum O_2 is significantly upraised in the region about $0.35 < r < 0.9$, beyond both ω_G and the continuum O, as shown in Fig. 7. The necessary condition for the existence of

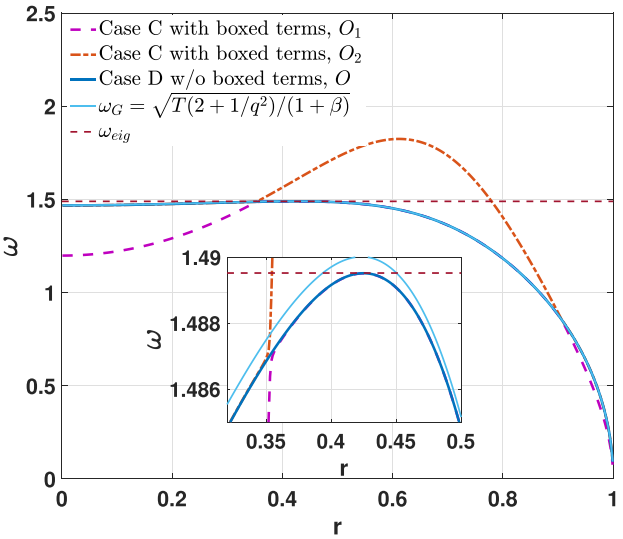

FIG. 7. The continuums for case C and case D under the equilibrium profile in Fig. 5. The eigenfrequency is chosen to be 1.4895.

global GAM is that there is a gap between the maximum of the GAM continuum O_2 and ω_G. In other words, the eigenfrequency of GGAM should be greater than the maximum of O_2 but less than the maximum of ω_G.[21]

IV. CONCLUSION

The global GAM is investigated by using the ideal MHD equations. The major results of this work can be summarized as the following three parts:

1. Using only the closed set of linearized ideal MHD equations, we concisely derived two mode equations describing ϕ_0 and ϕ_2, the $m=0$ and $m=2$ components of the GAM perturbed electrostatic potential, respectively. According to the two equations, the second order ODE determining the eigenfrequency and radial structure of the global GAM (GGAM) is presented in Eq. (22). The vortex equation, the current quasi-neutrality condition $\nabla \cdot \vec{J}$, and the ordering analysis are not additionally applied.
2. The high order boxed term in the coefficient of the second-order differential term in the ODE (22) will introduce another two continua, a higher frequency one O_3 and a relatively low frequency one O_1. Under some equilibrium profiles, for instance, in the reversed shear equilibrium profiles shown in Fig. 1 with $\beta(0) = 0.01$, the boxed term has a trivial effect on the GAM continuum O_2 and no qualitative effect on the eigenfrequency and radial structure of GGAM. There is a maximum of O_2 or the GAM continuum O in the case without the boxed term, and the eigenfrequencies are all beyond the maximum, as shown in Fig. 2. When the ODE is re-expressed in a standard form $f'' + cf = 0$, c remains positive in most regions except around r_0 (see Fig. 4), where r_0 is the point at which $\omega = \omega_G(r_0)$. The mode structures displayed in Fig. 3 are well explained when the eigenfrequency is much closer to the GAM continuum, the ODE has a local WKB solution with a much larger radial wave number k_r.
3. It is noted that for different equilibrium profiles, such as the one shown in Fig. 5 with an extremely low β $[\beta(0) = 0.001]$, although still reversed shear, c becomes negative in most regions away from r_0, leading to different mode structures in the case without boxed terms. We show that the boxed term plays an essential role and cannot be neglected. It upraises the GAM continuum remarkably and hence the gap between ω_G and the maximum of the GAM continuum disappears, as seen from Fig. 7. As a result, the solution illustrated in Fig. 6 does not exist now.

In the shear-reversed configurations, the GAM frequency naturally has a maximum, leading to the gap between the GAM continuum and the local GAM frequency, which leads to the existence of eigensolutions. While in the presence of energetic particles, the extremum in the GAM/EGAM continuum branches can come into being even for a monotonic $q(r)$.[11] It is important for us to understand the EGAMs, because the energetic particles need to be well confined and the bulk plasma heating efficiency needs to be improved in the magnetic confinement fusion devices.[22] Further investigation on the radial structure of EGAMs will be the scope of our future work.

ACKNOWLEDGMENTS

This work was supported by the National Natural Science Foundation of China under Grant No. 11675175, the China National Magnetic Confinement Fusion Energy Research Project under Grant No. 2015GB120005, the Fundamental Research Funds for the Central Universities under Grant No. DUT17RC(4)54, and the Innovative Program of Development Foundation of Hefei Center for Physical Science and Technology under Grant No. 2018CXFX009. This work was performed under the auspices of the U.S. Department of Energy by the Lawrence Livermore National Laboratory under Contract No. DE-AC52-07NA27344. LLNL-JRNL-844698

REFERENCES

[1]N. Winsor, J. L. Johnson, and J. M. Dawson, Phys. Fluids **11**, 2448 (1968).
[2]P. H. Diamond, S.-I. Itoh, K. Itoh, and T. S. Hahm, Plasma Phys. Controlled Fusion **47**, R35 (2005).
[3]A. Hasegawa and M. Wakatani, Phys. Rev. Lett. **59**, 1581 (1987).
[4]Z. Lin, T. S. Hahm, W. W. Lee, W. M. Tang, and R. B. White, Science **281**, 1835 (1998).
[5]F. L. Hinton and M. N. Rosenbluth, Plasma Phys. Controlled Fusion **41**, A653 (1999).
[6]K. Miki, Y. Kishimoto, N. Miyato, and J. Q. Li, Phys. Rev. Lett. **99**, 145003 (2007).
[7]H. L. Berk, C. J. Boswell, D. Borba, A. C. A. Figueiredo, T. Johnson, M. F. F. Nave, S. D. Pinches, S. E. Sharapov, and JET EFDA Contributors, Nucl. Fusion **46**, S888 (2006).
[8]N. Miyato, Y. Kishimoto, and J. Q. Li, Nucl. Fusion **47**, 929 (2007).
[9]Z. Gao, K. Itoh, H. Sanuki, and J. Q. Dong, Phys. Plasmas **15**, 072511 (2008).
[10]V. I. Ilgisonis, I. V. Khalzov, V. P. Lakhin, A. I. Smolyakov, and E. A. Sorokina, Plasma Phys. Controlled Fusion **56**, 035001 (2014).
[11]Y. I. Kolesnichenko, B. S. Lepiavko, and V. V. Lutsenko, Plasma Phys. Controlled Fusion **55**, 125007 (2013).
[12]T. Zhou and X. Wang, Nucl. Fusion **58**, 076006 (2018).
[13]O. P. Fesenyuk, Y. I. Kolesnichenko, H. Wobig, and Y. V. Yakovenko, Phys. Plasmas **9**, 1589 (2002).
[14]V. P. Lakhin, E. A. Sorokina, V. I. Ilgisonis, and L. V. Konovaltseva, Plasma. Phys. Rep. **41**, 975 (2015).
[15]H. Ren, Phys. Plasmas **19**, 094502 (2012).
[16]C. Wahlberg, Phys. Rev. Lett. **101**, 115003 (2008).
[17]C. Wahlberg and J. P. Graves, Plasma Phys. Controlled Fusion **58**, 075014 (2016).
[18]C. Wahlberg and J. P. Graves, Plasma Phys. Controlled Fusion **61**, 075013 (2019).
[19]O. P. Fesenyuk, Y. I. Kolesnichenko, and Y. V. Yakovenko Yu, Plasma Phys. Controlled Fusion **54**, 085014 (2012).
[20]H. Ren, D. Li, and P. K. Chu, Phys. Plasmas **20**, 072504 (2013).
[21]V. P. Lakhin and E. A. Sorokina, Phys. Lett. A **378**, 535 (2014).
[22]H. Wang, Y. Todo, M. Oasakabe, T. Ido, and Y. Suzuki, Nucl. Fusion **59**, 096041 (2019).